Biochimica et Biophysica Acta 1838 (2014) 2473–2483

Contents lists available at ScienceDirect

Biochimica et Biophysica Acta

journal homepage: www.elsevier.com/locate/bbamem

The role of ceramide chain length distribution on the barrier properties of the skin lipid membranes

E.H. Mojumdar, Z. Kariman, L. van Kerckhove, G.S. Gooris, J.A. Bouwstra *

Leiden Academic Center for Drug Research, Department of Drug Delivery Technology, Gorlaeus Laboratories, University of Leiden, Leiden, the Netherlands

ARTICLE INFO

Article history:
Received 6 December 2013
Received in revised form 25 April 2014
Accepted 19 May 2014
Available online 27 May 2014

Keywords:
Pig ceramides
Stratum corneum
Lipid mixtures
Infrared spectroscopy
X-ray diffraction

ABSTRACT

The skin barrier function is provided by the stratum corneum (SC). The lipids in the SC are composed of three lipid classes: ceramides (CERs), cholesterol (CHOL) and free fatty acids (FFAs) which form two crystalline lamellar structures. In the present study, we investigate the effect of CER chain length distribution on the barrier properties of model lipid membranes mimicking the lipid composition and organization of SC. The membranes were prepared with either isolated pig CERs (PCERs) or synthetic CERs. While PCERs have a wide chain length distribution, the synthetic CERs are quite uniform in chain length. The barrier properties were examined by means of permeation studies using hydrocortisone as a model drug. Our studies revealed a reduced barrier in lipid membranes prepared with PCERs compared to synthetic CERs. Additional studies revealed that a wider chain length distribution of PCERs results in an enhanced hexagonal packing and increased conformational disordering of the lipid tails compared to synthetic CERs, while the lamellar phases did not change. This demonstrates that the chain length distribution affects the lipid barrier by reducing the lipid ordering and density within the lipid lamellae. In subsequent studies, the effect of increased levels of FFAs or CERs with a long acyl chain in the PCERs membranes was also studied. These changes in lipid composition enhanced the level of orthorhombic packing, reduced the conformational disordering and increased the barrier of the lipid membranes. In conclusion, the CER chain length distribution is an important key factor for maintaining a proper barrier.

1. Introduction

The major role of the skin is to protect the body from the environment by providing an exceptionally efficient barrier. This physical barrier is located in the outer layer of the skin known as the stratum corneum (SC). The SC forms the rate limiting step for the penetration of drugs and other substances into the skin. Due to this role, it is important to understand the structure of the SC in relation to the skin barrier in more detail.

The composition of the SC is exclusive. It consists of dead flattened protein rich cells referred to as corneocytes being surrounded by intercellular lipids. These lipids greatly contribute to the barrier function of the skin. The main lipid classes in the SC are ceramides (CERs), cholesterol (CHOL) and free fatty acids (FFAs) in an approximately equimolar ratio [1–6]. In human and pig SC the lipids form two coexisting crystalline lamellar phases, referred to as the long periodicity phase (LPP) with a repeat distance of around 13 nm and the short periodicity phase (SPP) with a repeat distance of about 6 nm [7,8]. Apart from the lamellar phases, the arrangement of these lipids within the lipid lamellae, that is the compactness of the lipid chain packing, is also important for the skin barrier. This arrangement is referred to as the lateral packing. At skin temperature (~32 °C), the human SC lipids dominantly adopt a very dense orthorhombic packing. However, a small subpopulation of lipids is also present in a less dense hexagonal organization [7,9–12]. Both the lamellar phases and lateral packing are important and have been shown to play a role in the skin barrier function [13–16].

Further in-depth analysis of the SC lipid composition revealed different subclasses of CERs and the chain length distribution of CERs and FFAs in the SC. So far 12 different subclasses of CERs have been identified in the human SC, while in pig SC only 6 subclasses are present [1,4,5,17]. The CERs vary widely in their head group architecture and chain length distribution. Some of the CER classes have a very exceptional molecular architecture with a linoleic acid linked to a very long fatty acid chain. These CER subclasses are known as acyl CERs. The CERs are the key components in the skin barrier as they play a crucial role in maintaining this barrier [18]. In particular a reduction or complete abduction of the acyl CERs leads to an increased formation of the SPP and there are strong indications that this also leads to a reduced skin lipid barrier [13,19–21]. The FFAs present in native human SC are mainly saturated and range in chain length from C14 to C34 [20,22,23] with an average chain length between C20 and C22. It has been reported that the presence of FFAs enhances the formation of the orthorhombic lateral packing [24].

In our present study, we aimed to compare the barrier properties of lipid membranes prepared from isolated pig CERs (PCERs) with those

* Corresponding author at: Department of Drug Delivery Technology, Leiden Academic Center for Drug Research, Einsteinweg 55, 2333 CC Leiden, the Netherlands. Tel.: +31 71 527 4208; fax: +31 71 527 4565.
E-mail address: bouwstra@chem.leidenuniv.nl (J.A. Bouwstra).

http://dx.doi.org/10.1016/j.bbamem.2014.05.023
0005-2736/

prepared from synthetic CERs, in which the CER subclass composition mimics that of the PCER mixture. As each PCER subclass displays a multiple variation in chain length, in contrast to the synthetic CER composition having only 3 different chain lengths, a comparison between mixtures prepared with PCERs and synthetic CERs provides information on the role the chain length distribution plays in the skin lipid organization and barrier properties. In addition, the influence of increased levels of i) an acyl CER subclass, known as CER EOS (esterified -hydroxysphingosine, an acyl CER, see Fig. 1), and ii) FFAs on the barrier properties have also been examined. To accomplish our endeavors, we used small angle X-ray diffraction (SAXD) to elucidate the lamellar phases and Fourier transform infrared spectroscopy (FTIR) to examine the lateral packing, the conformational ordering and the mixing properties of the lipid mixtures. *In vitro* permeation studies were performed using a lipid model membrane cast on a porous support, referred to as the stratum corneum substitute (SCS) [25,26]. As model drug we used hydrocortisone.

2. Materials and method

2.1. Materials

Five subclasses of synthetic CERs were used in our studies. These are an ester linked omega-hydroxyl acyl chain (30 carbons in the acyl chain (C30)) with a sphingosine chain (C18) referred to as CER EOS (C30), a non-hydroxy acyl chain (C24) linked to a sphingosine base (C18) referred to as CER NS (C24), a non-hydroxy acyl chain (C24 or C16) linked to a phytosphingosine base referred to as CER NP (C24) and CER NP (C16), respectively, an alpha-hydroxy acyl chain linked to a sphingosine base referred to as CER AS (C24), and an alpha-hydroxy acyl chain (C24) linked to a phytosphingosine base referred to as CER AP (C24). The number between parentheses indicates the number of carbon atoms present in the acyl chain of the CER subclass. The molecular structure of the various synthetic CERs is provided in Fig. 1. All the CERs were kindly provided by Evonik (Essen, Germany). The FFAs with a chain length of C16:0, C18:0, C20:0, C22:0, C23:0, C24:0 or C26:0 are obtained from Sigma-Aldrich Chemie GmbH (Schnelldorf, Germany). CHOL, trypsin (type III, from bovine pancreas) and trypsin inhibitor (type II-S from soybean) were also purchased from Sigma-Aldrich Chemie GmbH (Schnelldorf, Germany). The perdeuterated FFAs with chain lengths of C16:0 and C22:0 and hydrocortisone were purchased from Larodan (Malmo, Sweden). The perdeuterated FFAs with chain lengths of C14:0, C18:0, and C20:0 were obtained from Cambridge Isotope Laboratories (Andover MA, USA). Nucleopore polycarbonate filter disks (pore size 50 nm) were obtained from Whatman (Kent, UK). All solvents were of analytical grade and supplied by Labscan (Dublin, Ireland). The water was of Millipore quality.

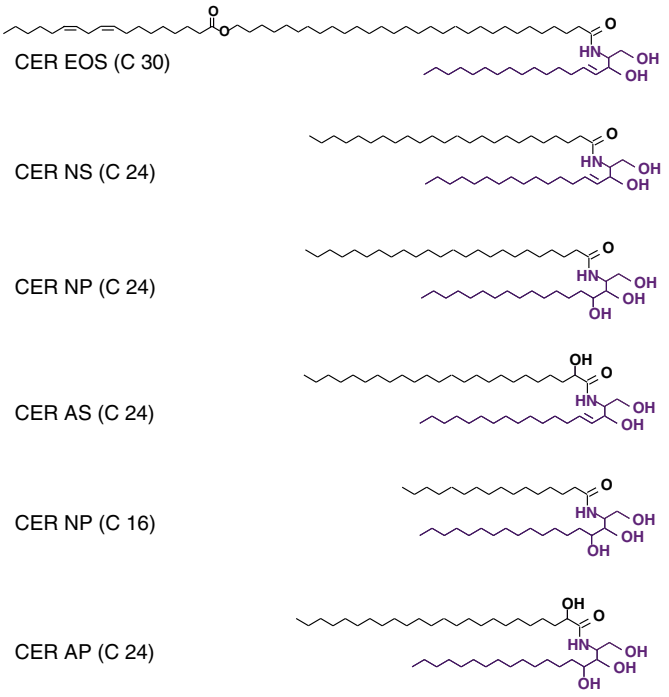

Fig. 1. Molecular structure of the synthetic CERs used in the present study. The CER consists of an acyl chain ranging from 24 to 30 carbons linked to a sphingoid base through an amide linkage.

2.2. Isolation and extraction of PCER

Fresh pig skin was obtained from the Central Veterinary Institute in Lelystad in the Netherlands. First, the hairs were removed with a razor blade. Then the pig skin was defatted and dermatomed at a thickness of 600 μm. The SC was isolated by trypsin digestion (0.1% in a phosphate-buffered saline solution) as described previously [27]. SC lipids were extracted using the method of Bligh and Dyer [28]. Briefly, first a series of chloroform:methanol extractions in various ratios (1:2, 1:1 and 2:1 v/v) was performed for 1 h at 37 °C. The extracts were then combined and treated with 2.5% KCl in demi-water to create an aqueous phase. The organic phase was collected, evaporated using a rotary evaporator and subsequently applied onto a silica gel 60 column after being redissolved in a suitable volume of chloroform:methanol (2:1). Then the various lipid classes were eluted sequentially using a series of solvent mixtures as published previously [27]. The lipid composition of the collected fractions was examined by one dimensional high performance thin layer chromatography (HPTLC), as described previously [27]. Then the fractions that contained only CERs were combined and the composition was analyzed. For quantification of the CER subclasses, HPTLC was performed: authentic standards (mixtures of 7 different CERs) and the isolated PCERs were run in parallel. To perform the quantification 12 different amounts of the CER standard solution and isolated PCER solution were applied on the plate. The quantification was performed after charring, using a photodensitometer with peak integration (Biorad, GS 800). The linear part of the calibration curves were used for calculating the relative levels of the PCER subclasses.

2.3. Mass spectrometry analysis

The PCERs were further analyzed by liquid chromatography coupled to mass spectrometry (LC/MS) in order to investigate the chain length distribution. A detailed description of the lipid analysis is given elsewhere [17]. In short, the PCER sample was redissolved in chloroform: methanol:heptane (2.5:2.5:95) to a final concentration of 1 mg/mL. 10 μL of sample was injected using an HPLC system (Waters, Thermo, Finnigan, San Jose, CA). The HPLC was coupled to a mass spectrometer (TSQ Quantum, Thermo, Finnigan, San Jose, CA) to analyze the PCER composition. The separation of the PCER was achieved by using a normal phase column (PVA-sil, YMC, Kyoto, Japan) while analyzing in positive ion mode. The software Xcalibur was used for data acquisition.

2.4. Compositions of stratum corneum substitute (SCS)

For the preparation of the SCS, synthetic CERs or PCER, CHOL and FFAs were used. The two compositions of the synthetic CERs with their corresponding molar ratios are provided in Table 1. One of these compositions is based on a CER subclass composition of pig SC reported earlier [27,29] and is referred to as $CER^{control}$. The other synthetic CER composition mimics the composition of the PCERs isolated in the present study and is referred to as CER^{spig}. The composition of the FFA mixture was comprised of seven different FFAs. The name, chain length and the molar ratios of the FFA mixture are provided in Table 1. This FFA composition is based on that reported for human SC [30]. In a few FTIR experiments, the protonated FFAs were replaced by deuterated FFAs

Table 1
The composition and molar ratios of the synthetic CERs and FFAs used in the current study are presented in the table. The synthetic CER mixture used in previous studies ($CER^{control}$) and the synthetic CER mixture (CER^{spig}) mimicking the subclass composition of isolated pig CERs used in the present study are provided. In addition the FFAs molar ratio is given.

CER name and chain length	Molar ratio (%) in $CER^{control}$	Molar ratio (%) in CER^{spig}	FFA name and chain length	Molar ratio (%)
CER EOS (C30)	15	13.8	Palmitic acid (c16)	1.8
CER EOP (C30)	–	0.9	Stearic acid (c18)	4.0
CER NS (C24)	51	44.2	Arachidic acid (c20)	7.7
CER NP (C24)	16	8.8	Behenic acid (c22)	42.6
CER AS (C24)	4	5.9	Tricosylic acid (c23)	5.2
CER NP (C16)	9	16.8	Lignoceric acid (c24)	34.7
CER AP (C24)	5	9.7	Cerotic acid (c26)	4.1
Total	100	100	Total	100

(DFFAs) with the following composition: C16:0, C18:0, C20:0, C22:0 and C24:0 at molar ratios of 1.8, 4.0, 7.6, 47.8 and 38.8 respectively. In total, six different model membrane systems have been prepared. The detailed composition and the molar ratios of these model types are provided in Tables 1 and 2.

2.5. Preparation of the SCS for diffusion and SAXD studies

For each of the lipid mixtures the appropriate amount of individual lipids was combined, after which the organic solvent chloroform:methanol (2:1) was evaporated under a flow of nitrogen. Then the lipids were redissolved in a hexane:ethanol (2:1) solution and used to prepare the SCS. To spray the lipid mixtures on Whatman nucleopore polycarbonate filters disks, a Camag Linomat IV (Muttenz, Switzerland) was used with an extended y-axis arm [31]. A Hamilton syringe (100 μL) was inserted in the Linomat and used to spray a selected volume of sample solution from a distance of approximately 1 mm onto the porous filter substrate under a gentle stream of nitrogen flow. With the y-axis arm, the Linomat is capable of spraying lipids in a square shape (8 by 8 mm), by a continuous zigzag movement. The spraying flow rate was set to 5.0 μL/min and 0.9 mg of lipids per membrane was sprayed. After spraying, the SCS was equilibrated for 12 min between 70 and 80 °C depending on the selected lipid composition. After equilibration, the membranes were gradually cooled to room temperature and measured by SAXD.

2.6. Sample preparation for FTIR studies

The preparation method differed slightly from the above described method. 1.5 mg of lipids was dissolved in a chloroform:methanol (2:1) solution. The spraying area was 1×1 cm^2 on a ZnSe (zinc selenide) window. The samples were equilibrated for about 10 min at approximately 80 °C and cooled gradually to room temperature. Subsequently, the lipid layers were covered with 25 μL deuterated acetate buffer (pH 5.0) and stored at 37 °C for 15 h to fully hydrate the sample. Although the FTIR sample preparation is slightly different compared to SCS membrane preparation, for clarity the SCS term will be used throughout the paper.

2.7. SAXD methodology

SAXD was used to examine the lamellar organization. The scattering intensity I (in arbitrary units) was measured as a function of the scattering vector q (in reciprocal nm). The latter is defined as $q = (4\pi\sin\theta) / \lambda$, in which θ is the scattering angle and λ is the wavelength. From the positions of a series of equidistant peaks (q_n), the periodicity, or d-spacing of a lamellar phase was calculated using the equation $d = 2n\pi / q_n$, with n being the order number of the diffraction peak. One-dimensional intensity profiles were obtained by the transformation of the 2D SAXD detector pattern from Cartesian (x,y) to polar (ρ,θ) coordinates and subsequently integrating over θ. All measurements were performed at the European Synchrotron Radiation Facility (ESRF, Grenoble) using station BM26B. The X-ray wavelength and the sample-to-detector distance were 0.1033 nm and 2 m respectively. Diffraction data were collected on a PILATUS 1 M detector with 1043×981 pixels of 172 μm spatial resolution. The spatial calibration of this detector was performed using silver behenate ($d = 5.838$ nm for AgBeh). The SCS (prepared on a polycarbonate filter disk) was mounted parallel to the primary beam in a sample holder with mica windows. The diffraction data were collected for 10 min at 25 °C.

2.8. FTIR methods

The FTIR instrument consists of a BIORAD FTS4000 FTIR spectrometer (Cambridge MA, USA) equipped with a broad-band mercury cadmium telluride detector, cooled by liquid nitrogen. The sample cell was closed by two ZnSe windows. The sample was under continuous dry air purge starting 30 min before the data acquisition. The spectra were collected in transmission mode with a co-addition of 256 scans at 1 cm^{-1} resolutions during 4 min. In order to detect phase transitions, the sample temperature was increased at a heating rate of 0.25 °C/min resulting in a 1 °C temperature rise per recorded spectrum. The spectra were collected between 0 °C and 90 °C and deconvoluted using a half-width of 4 cm^{-1} and an enhancement factor of 1.7. The software used for data reduction was Win-IR pro 3.0 from Biorad. The linear regression curve fitting method was used to determine the transition temperature of the lipid mixtures. The CH_2 symmetric stretching vibration frequencies in the spectra were used to study the orthorhombic to hexagonal phase transition in the temperature range of 20–40 °C and the hexagonal to liquid phase transition in the temperature range between 50 and 80 °C. The CH_2 rocking vibrations were used to study the orthorhombic to hexagonal phase transition into more details.

2.9. Diffusion setup

Diffusion studies were performed with PermeGear inline diffusion cells (Bethlehem PA, USA) with a diffusion area of 0.282 cm^2. The SCSs

Table 2
The various lipid mixtures with their composition and molar ratios used to prepare the SCSs. The lipid lamellar organization with their corresponding repeat distances is presented. The lipid lateral packing and the wavenumbers of the CH_2 stretching vibrations indicative for the conformational ordering are also given in the table. The steady state flux of the model drug hydrocortisone across the SCSs with their associated standard deviation is also shown.

Denotation in the text	Lipid composition and molar ratio	Lamellar organization (25 °C)	Repeat distance (nm)	Lateral packing (32 °C)	Conformational ordering (32 °C)	Steady state flux (μg/cm^2/h)
$SCS^{control}$	$CER^{control}$/CHOL/FFA (1:1:1)*	LPP, SPP	12.1, 5.3	Orthorhombic	2850.1	0.04 ± 0.01
SCS^{spig}	CER^{spig}/CHOL/FFA (1:1:1)*	LPP, SPP	12.1, 5.3	Orthorhombic	2849.9	0.06 ± 0.03
$pigSCS^{111}$	PCER/CHOL/FFA (1:1:1)	LPP, SPP	12.5, ~5.7	Hexagonal	2850.9	0.76 ± 0.14
$pigSCS^{112}$	PCER/CHOL/FFA (1:1:2)	SPP	5.8	Slightly orthorhombic	2850.7	0.40 ± 0.01
$pigSCS^{EOS111}$	PCER + 20 mol% CER EOS/CHOL/FFA (1:1:1)**	LPP, SPP	13.1, ~5.8	Slightly orthorhombic	2851	0.31 ± 0.07
$pigSCS^{EOS11}$	PCER + 20 mol% CER EOS/CHOL (1:1)	LPP, SPP	13.1, ~4.4	Slightly orthorhombic	2850.7	0.54 ± 0.07

* The synthetic CER mixture was prepared based on CER molar ratios presented in the Table 1.
** The mixture was prepared using PCERs with an addition of 20 mol% of CER EOS. The CER, CHOL and FFA molar ratios are equimolar.

were mounted in the diffusion cells with magnetic stirrers. Phosphate-buffered saline (PBS) served as the acceptor phase solution during the permeation studies. The phosphate-buffered saline (PBS) solution was prepared by adding NaCl, Na_2HPO_4, KH_2PO_4 and KCL in MQ water in concentrations of 8.13, 2.87, 0.20 and 0.19 g/L respectively; the buffer was adjusted to a pH of 7.4, filtrated and degassed for 15 min with helium. The donor phase solution of the diffusion cells was prepared with the model drug hydrocortisone (MW = 364 g) dissolved in acetate buffer (NaAc * $3H_2O$ solution acidified with acetic acid (CH_3CO_2H) to pH 5) and 1.4 mL of hydrocortisone solution was applied in the donor compartment at a saturated concentration of 0.3 mg/mL. A saturated concentration was used to obtain a maximum thermodynamic activity. The donor compartment was closed with an adhesive tape for maintaining occlusive conditions throughout the experiment. The molecular structure of the drug compound hydrocortisone is presented in Fig. 2A.

The acceptor phase with PBS (pH 7.4) was perfused at a flow rate of approximately 2 mL/h with a flow pump (Ismatec IPC pump; IDEX Health & Science GmbH, Germany) and the acceptor compartments were stirred with the magnetic stirrers at 160 rpm to prevent accumulation of the model drug. A fraction collector (Isco Retriever IV; Teledyne Isco, USA) was used to collect the acceptor fluid in 10 mL glass vials each hour. The exact volume per collected fraction was determined by weighing. The temperature of the diffusion cells during permeation was controlled at physiological human skin temperature of approximately 32 °C by a thermo-stated water bath (Thermostat from Lauda Dr. Wobser GmbH; Lauda-Koenigshofen, Germany). The steady state flux (Jss) values between time intervals of 5 and 15 h were calculated from the cumulative plot flux values of the permeating compound. The slope of the linear part of the cumulative plot represents the steady state flux. A schematic drawing of the diffusion setup is presented in Fig. 2B.

2.10. HPLC method

Quantification of the drug compound hydrocortisone was carried out by high performance liquid chromatography (HPLC) analysis. The HPLC system consisted of a Spectra system UV2000 detector (Thermo Separation Products Inc., California, USA), a high precision pump model 300 (Thermo Separation Products Inc., California, USA) and a solvent recycler, complemented with an auto injector (Gilson 234 Autoinjector; Gilson Inc., Middleton, USA). The C18 reversed phase column (Alltima, 50 μm id, 125 × 4.0 mm) was used during the experiment. The mobile phase used for the HPLC analysis contained helium degassed mixtures of acetonitrile:Millipore water at a 40:60 (v/v) ratio. The UV-detection wavelength of 243 nm was used for a hydrocortisone drug molecule. The flow rate of the mobile phase was set to 1 mL/min. Series of calibration samples were run in parallel with each series of the permeation samples to separate and quantify the drug compound. The Software ADchrom was used to analyze and integrate the HPLC data.

2.11. Statistical analysis

Statistical analysis was performed using the Excel spreadsheet version 2010. Unpaired two-tailed *T*-test and one-way ANOVA were performed, both with a significance level set at $P < 0.05$.

3. Results

3.1. CER composition: quantification and chain length distribution in PCERs

After isolation of PCERs from pig SC, the composition of the PCERs was determined by HPTLC. Fig. 3 shows the molar composition of CER subclasses in the isolated PCER mixture. CER NS is present at a high level, namely 44 mol%, while the abundance of CER EOS is 13 mol%. A small level of CER EOP is also present. This composition of PCERs is similar as reported in the literature, although the most hydrophilic CER subclasses are slightly more abundantly present compared to the previous published composition [32]. To obtain information on the chain length distribution of the various CER subclasses, LC/MS was performed and the results are provided in Fig. 4. In the 3-D mass spectrum, the same subclasses of PCER mixture are shown confirming the HPTLC results. Furthermore, the LC/MS results also show a large distribution in CER chain lengths. The most abundant chain lengths are observed for the CER NS subclass ranging from C32 to C40 (total chain length: sphingoid base + acyl chain). The shorter chain lengths are observed most abundantly in the CER AdS and CER AS subclasses with a total chain length of C34 for CER AdS and C33–C34 for the CER AS (marked by x in the chromatogram).

3.2. The CER chain length distribution affects the lipid barrier function

To investigate the effect of lipid composition on the skin barrier, diffusion studies were performed using hydrocortisone as model drug. Fig. 5 displays the mean flux profiles of all the SCSs used in our study. The steady state fluxes of all SCSs with their standard deviation are provided in Table 2.

First, we will focus on the SCSs prepared with the synthetic CER mixtures. The hydrocortisone steady state flux across $SCS^{control}$ (prepared with the $CER^{control}$ we used in previous studies), revealed a steady state flux of 0.04 ± 0.01 μg/cm²/h. When comparing this mixture with the SCS^{spig} prepared with the CER^{spig}, the hydrocortisone steady state flux is 0.06 ± 0.03 μg/cm²/h which is not significantly different from that of the $SCS^{control}$. In parallel, we measured the hydrocortisone flux across SCS prepared from PCERs. The steady state flux of the $pigSCS^{111}$ prepared with PCER/CHOL/FFA (1:1:1) is significantly increased to a value of 0.76 ± 0.14 μg/cm²/h, which is approximately 12 times higher compare to the SCS^{spig}.

3.3. The addition of CER EOS and/or FFA reduces the hydrocortisone flux

We also examined the effect on the hydrocortisone flux after increasing the levels of CER EOS in the SCS. The $pigSCS^{EOS11}$ prepared with (PCER + 20 mol% additional CER EOS)/CHOL (1:1) resulted in a steady state flux of 0.54 ± 0.07 μg/cm²/h. The addition of FFA to this mixture ($pigSCS^{EOS111}$) resulting in a composition of (PCER + 20 mol% CER EOS)/CHOL/FFA (1:1:1) reduced the steady state flux further to 0.31 ± 0.07 μg/cm²/h. A further increase of FFA in the PCER/CHOL/FFA mixture resulting in a molar ratio 1:1:2 ($pigSCS^{112}$) also reduced the steady state flux to 0.40 ± 0.01 μg/cm²/h compared to the steady state hydrocortisone flux obtained with $pigSCS^{111}$.

As we obtained differences in the hydrocortisone steady state flux across the various SCSs indicating differences in lipid organization, we decided to study the lipid organization of these SCSs. For this reason SAXD and FTIR studies were performed.

3.4. Lamellar phase behavior of the various lipid mixtures

SAXD was used to study the lamellar organization of the SCSs. The detected lipid lamellar phases with their corresponding repeat distances are provided in Table 2 for various lipid mixtures. First the SCSs prepared from synthetic CERs are described (see Fig. 6A, top — $SCS^{control}$, bottom — SCS^{spig}). The SCSs prepared with synthetic CERs, either $SCS^{control}$ or SCS^{spig}, displayed two lamellar phases with repeat distances of 12.1 and 5.3 nm being the LPP and SPP, respectively. The peaks at q = 0.52, 1.05, 1.57 and 2.1 nm^{-1} indicate the 1st, 2nd, 3rd and 4th order peaks attributed to the LPP with a repeat distance of 12.1 nm whereas the peaks at q = 1.18 and 2.36 nm^{-1} indicate the 1st and 2nd order peaks attributed to the SPP respectively with a repeat distance of 5.3 nm. No significant differences were noticed between the diffraction profiles of these two SCSs.

When focusing on the SCSs prepared with isolated PCERs, we first present the results obtained with $pigSCS^{111}$ (Fig. 6B). The diffraction

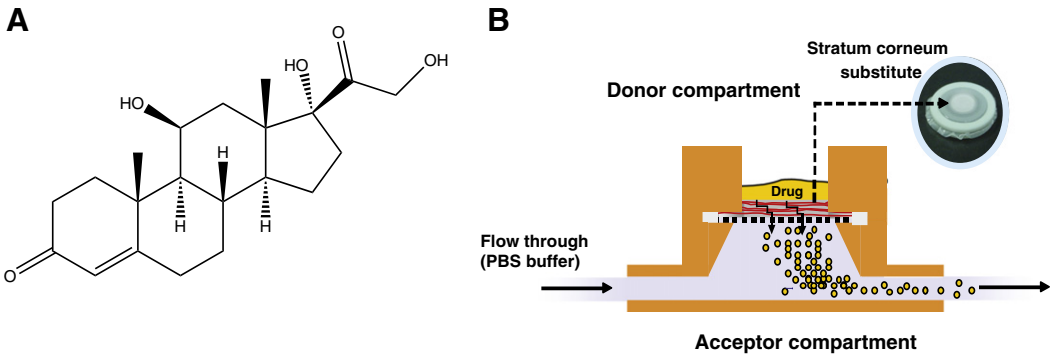

Fig. 2. (A) The molecular structure of the drug compound hydrocortisone (MW = 364 g) used for permeation studies. (B) A schematic drawing of the diffusion cell.

patterns indicate the presence of the LPP and SPP with repeat distances of 12.5 and approximately 5.7 nm, respectively. In this pattern, the 1st and 3rd order peaks of the LPP located at $q = 0.50$ and 1.50 nm^{-1} are clearly visible along with the peak from crystalline CHOL ($q = 1.8$ nm^{-1}). The 2nd order LPP peak is visible as a small shoulder on the left side of the 1st order SPP peak positioned at $q = 1.10$ nm^{-1}. In additional studies we elevated either the FFA level or the CER EOS level. When focusing on an increased level of FFA, we did notice changes in the lamellar phases. In the $pigSCS^{112}$ the lipids form only the SPP with a repeat distance of 5.8 nm (Fig. 6C). The diffraction peaks at $q = 1.07$, 2.15 and 3.22 nm^{-1} indicate the 1st, 2nd and 3rd order peaks of SPP respectively. Two SCSs were examined with an addition of 20 mol% CER EOS, i.e., $pigSCS^{EOS11}$ and equimolar $pigSCS^{EOS111}$ (Fig. 6D, top — $pigSCS^{EOS111}$, bottom — $pigSCS^{EOS11}$). In both SCSs, the LPP was abundantly present with a slightly increased repeat distance to approximately 13.1 nm compared to the $pigSCS^{111}$ (not enriched with CER EOS). In the $pigSCS^{EOS11}$, the lipids mainly adopt the LPP. As the 3rd order diffraction peak attributed to the LPP is quite broad, most probably this peak is also attributed to another phase indicating a slight phase separation. In the diffraction profile of the $pigSCS^{EOS111}$ we notice an asymmetric 2nd order diffraction peak of the LPP, suggesting that not only the LPP but also the SPP is formed (peak positioned at $q = \sim 1.07$ nm^{-1}, shoulder indicating the 1st order diffraction peak).

3.5. Conformational ordering and lateral packing of the lipid mixtures determined by FTIR

Besides the lamellar phases, the lateral packing and conformational disordering may also play a role in the barrier properties of the SCS. To investigate the lateral packing and conformational disordering the SCSs were examined by FTIR.

3.5.1. Conformational ordering

The CH_2 symmetric stretching frequency provides information about the conformational ordering of the lipid tails in the mixtures. A low (~2848 cm^{-1}) wavenumber of the CH_2 symmetric stretching vibrations indicates the presence of a highly ordered lipid organization (either hexagonal or orthorhombic), while a high (~2853 cm^{-1}) wavenumber indicates a liquid disordered phase [33]. The CH_2 symmetric stretching position in the FTIR spectrum is examined as a function of temperature and the results are provided in Fig. 7: two clearly distinct groups of stretching vibrations are detected. Two spectra with low CH_2 stretching frequencies are obtained with $SCS^{control}$ and SCS^{spig}: at 10 °C CH_2 stretching frequencies of around 2849.5 cm^{-1} are observed. The frequencies gradually shift to higher values until 30 °C. The low values indicate conformational ordering of the lipids in the SCS in this temperature range. A further increase in temperature from 30 to 40 °C results in a shift of CH_2 symmetric frequency from 2849.5 to 2851.3 cm^{-1} for the $SCS^{control}$ and 2850.5 cm^{-1} for the SCS^{spig}. These changes are based on a phase transition from orthorhombic to a hexagonal lateral packing (see below). Between 40 and 60 °C a further gradual increase in frequency was observed indicating an increased conformational disordering of the chains. A subsequent further increase in temperature from 60 to 80 °C results in a large frequency shift from 2851.3 to 2853.3 cm^{-1} for the $SCS^{control}$ and 2850.5 to 2853.4 cm^{-1} for the SCS^{spig}, demonstrating the formation of a liquid phase in this temperature range.

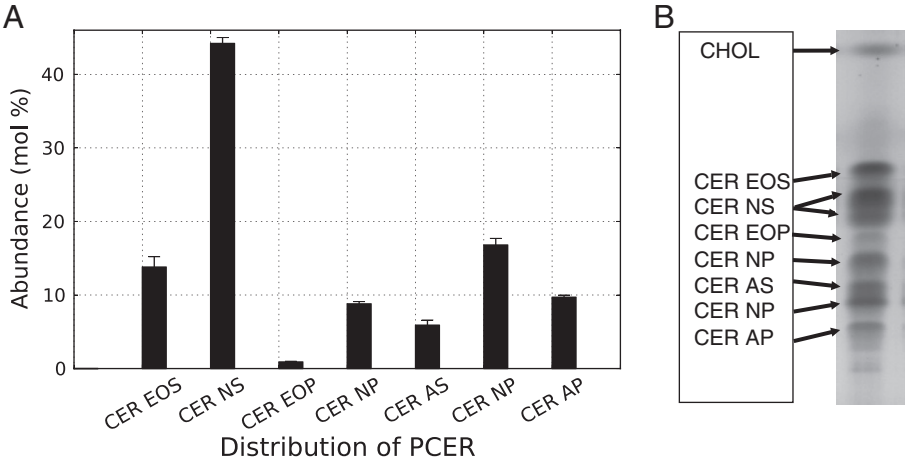

Fig. 3. High performance thin layer chromatography of isolated PCERs. (A) The CER subclasses with their corresponding name and molar ratios are shown for the PCER mixture. (B) The HPTLC plate shows the corresponding bands of the isolated PCER.

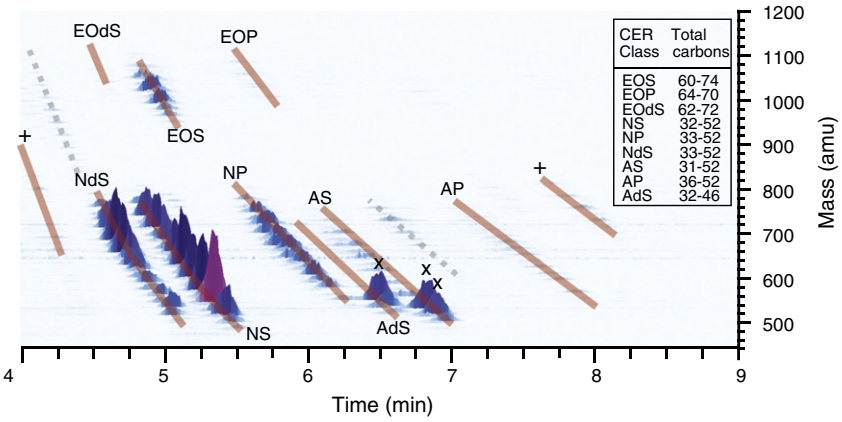

Fig. 4. 3-D multi-mass chromatogram for PCER analysis showing different subclasses of PCER and their chain length distribution. The labeled '+' signs are unknown lipid classes and the 'x' indicates the increased abundance of the very short CERs in the pig SC. The PCERs prevail with a wider chain length distribution compared to the synthetic CERs.

The SCSs prepared with PCERs display the higher values of the CH_2 symmetric stretching frequencies. In the spectrum of pigSCS^{111} at 10 °C the CH_2 symmetric frequency is located at 2850.0 cm^{-1}. This is at higher values than in the spectra of the mixtures prepared with the synthetic CERs. Between 10 °C and 50 °C a gradual increase in the CH_2 symmetric frequency is observed from 2850.0 cm^{-1} to 2851.2 cm^{-1}. Increasing the temperature above 50 °C results in a large shift of the CH_2 symmetric stretching frequencies to 2853.2 cm^{-1} suggesting the presence of a liquid phase. The spectrum of the pigSCS^{11} (equimolar PCER/CHOL mixture) has an initial CH_2 symmetric frequency of 2850.6 cm^{-1} at 10 °C and a gradual increase is observed until 50 °C with a CH_2 symmetric frequency of 2851.4 cm^{-1}. Beyond 50 °C, a transition occurred with a frequency of 2853.4 cm^{-1} at 85 °C, indicative of the presence of a liquid phase.

In addition, we also studied the effect of an increased level of either CER EOS or FFA in the mixtures. First we will present the studies with SCS with increased EOS levels, namely pigSCS^{EOS111} and pigSCS^{EOS11}. The FTIR spectra of both SCS exhibit a CH_2 symmetric stretching frequency of 2850.3 cm^{-1} at 10 °C. Increasing the temperature of the pigSCS^{EOS111}, the frequency gradually shifts from 2850.3 to 2851.3 cm^{-1} at 60 °C. Subsequently a clear shift is noticed between 60 and 80 °C with a final CH_2 symmetric frequency of 2853.6 cm^{-1} at 80 °C. For the pigSCS^{EOS11}, the symmetric stretching frequency remains similar until 50 °C after which from 50 to 80 °C a symmetric frequency shift occurs from 2851.2 to 2853.7 cm^{-1} indicating the transition from an ordered to a disordered liquid phase. The stretching frequency of the pigSCS^{112} starts with 2850.1 cm^{-1} at 10 °C and increased gradually until 65 °C to 2851.7 cm^{-1}. A further increase in temperature results in an ordered–disordered transition with a CH_2 symmetric frequency of 2853.3 cm^{-1} at 85 °C.

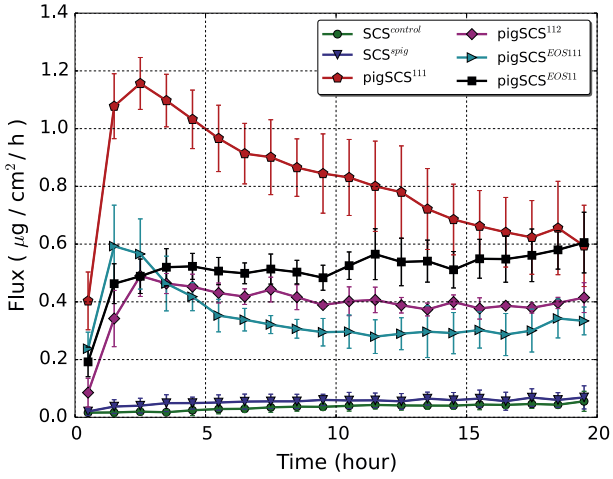

Fig. 5. Flux profiles of hydrocortisone across SCSs prepared from various lipid mixtures. The SCSs are prepared from either isolated PCERs or synthetic CERs. Figure legend shows the denotation of different model lipid mixtures used in permeation studies. For the detailed compositions and molar ratios, see Tables 1 and 2. The SCSs prepared from PCERs prevail with a higher permeation flux than the SCSs prepared from synthetic CERs.

3.5.2. Lateral packing

The FTIR rocking frequencies provide information on the lateral packing of the lipid chains. When the lipid tails in the mixtures adopt an orthorhombic lateral organization, the contours of the rocking vibrations in the FTIR spectrum are characterized by a doublet with rocking frequencies at approximately 720 and 730 cm^{-1}. This doublet is caused by the interactions of the adjacent lipid chains *via* a short range coupling [34]. On the contrary, when the lipids adopt a hexagonal phase, instead of a doublet a singlet is observed at 721 cm^{-1} in the FTIR spectra. Due to the less dense packing in the hexagonal organization no short range coupling occurs. The CH_2 rocking frequencies in the FTIR spectrum of all model lipid mixtures are shown in the temperature range from 20 to 40 °C in Fig. 8. The lipid lateral packing of all the lipid mixtures are provided in Table 2.

The FTIR spectra of the SCS^{control} and SCS^{spig} show a strong doublet in the rocking vibration frequencies at approximately 720 and 731 cm^{-1} at 20 °C, indicative of the presence of the highly ordered orthorhombic packing (Fig. 8A and B). A gradual increase in temperature results in a gradual reduction in the intensity of the 730 cm^{-1} rocking frequency. At 40 °C only a singlet is observed, indicating that the orthorhombic phase disappeared.

The rocking vibrations in the spectrum of the pigSCS^{111} exhibits the presence of a broad intense contour at approximately 720 cm^{-1} at 20 °C in the spectrum revealing the presence of mainly a hexagonal packing (Fig. 8C). However, a weak shoulder is also observed at ~730 cm^{-1} suggesting that a small population of lipids adopts an orthorhombic organization at this temperature. When raising the temperature, the weak shoulder starts to disappear and the contour becomes a singlet at around temperature of 30 °C. To examine the effect of the level of FFA in the SCS on its lateral packing, we also measured the pigSCS^{11} and pigSCS^{112}. In the spectrum of the pigSCS^{11} a single rocking vibration is observed in the whole temperature range studied and therefore in this mixture, only a hexagonal lateral organization is present (Fig. 8D). In the pigSCS^{112}, the spectrum of this SCS adopts a doublet in the rocking FTIR spectra at 20 °C at frequencies of 731 and 720 cm^{-1} (Fig. 8E). This 731 cm^{-1} contour does not reduce in intensity when increasing the temperature to 40 °C.

When focusing on the effects of CER EOS levels, we examined the pigSCS^{EOS11} and pigSCS^{EOS111}. In the spectrum of pigSCS^{EOS11} a broad

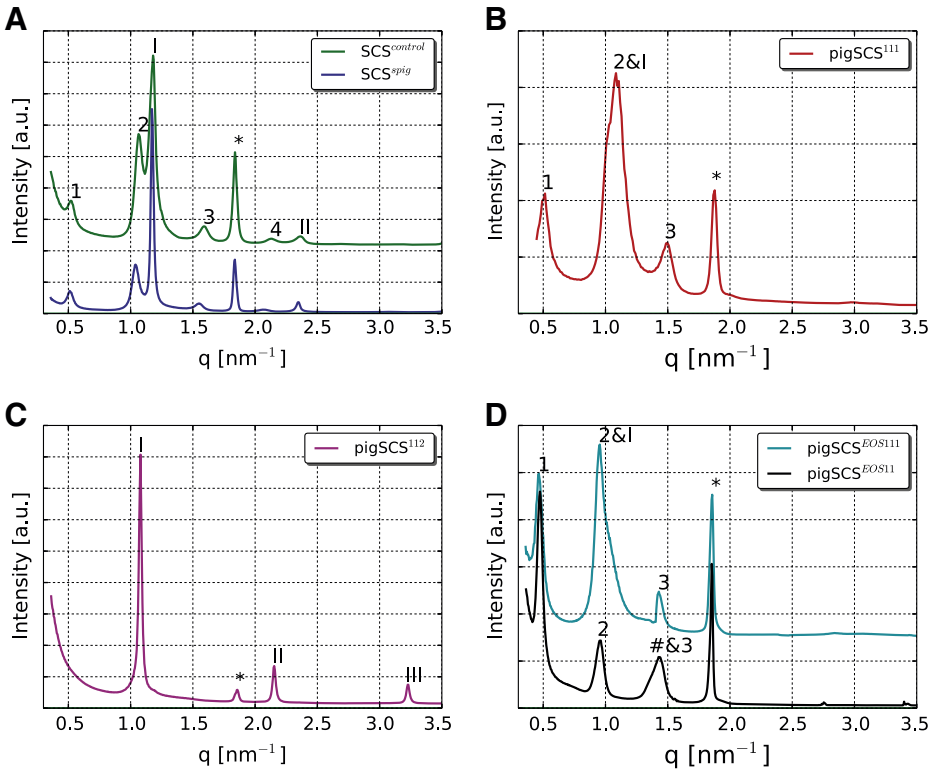

Fig. 6. SAXD diffraction profile of different SCSs used in our study. The figure legend describes the denotation of the different lipid mixtures prepared. The detailed composition and molar ratios are given in Tables 1 and 2. In the SAXD profiles, the Arabic numbers (1, 2, 3…) indicate the different diffraction orders of the LPP. The Roman numbers (I, II…) indicate the diffraction orders attributed to the SPP. Panel A — top: SCS^{control} and bottom: SCS^{spig}; panel D — top: pigSCS^{EOS111} and bottom: pigSCS^{EOS11}. The peaks originating from crystalline CHOL domains are indicated by an asterisk (*). The relatively shorter phase observed in panel D (bottom) is indicted by a hash (#) sign.

intense contour similar to that in the spectrum of the pigSCS^{111} is observed in the FTIR rocking vibrations at 20 °C at approximately 720 cm^{-1} (Fig. 8F), suggesting the presence of mainly a hexagonal phase, while a small population of lipids adopts an orthorhombic lateral organization (shoulder at around 730 cm^{-1}). Unlike the pigSCS^{111} mixture, the 730 cm^{-1} contour does not vanish upon heating until 40 °C. In the spectrum of pigSCS^{EOS111} a strong doublet is observed in the rocking vibration frequencies at 720 and 731 cm^{-1} at 20 °C (Fig. 8G). A gradual increase in temperature beyond 20 °C results in a collapse of the doublet in this mixture: one singlet is observed at 40 °C indicating the absence of the orthorhombic lateral packing.

In order to investigate whether phase separation occurs between CER and FFA in the SCS, the protonated FFA was replaced by DFFA and the splitting of the FTIR scissoring mode was examined. The use of DFFA allows us to monitor whether CER and FFA participate in one lattice or phase separate. When the DFFA and CER participate in an orthorhombic lattice, due to the difference in frequencies, the CH_2 and CD_2 cannot interact with each other. As a result, no or only a weak doublet is observed in the FTIR spectrum [35]. We particularly focused on two SCSs: the CD_2 scissoring vibrations in pigSCS^{EOS111} and pigSCS^{112}, both exhibiting an orthorhombic lateral packing. The results are provided in Fig. 9A and B. In the spectrum of the pigSCS^{EOS111} a weak doublet is detected at low temperature (10 °C) which dissolves when the temperature is increased. The scissoring vibration turns into a singlet at around 20 °C and indicates that DFFA and CER are participating in the same lattice. In case of pigSCS^{112}, the doublet in the scissoring mode is stronger at low temperatures and remains visible until 40 °C, suggesting phase separation of FFA in an orthorhombic lattice.

4. Discussion

The aim of our current study is to examine whether SCSs prepared from isolated PCERs do have a difference in permeability compared to membranes prepared from synthetic CERs and whether the differences in permeability can be explained by differences in the lipid composition and subsequent organization. Furthermore, the effect of increased levels of FFAs and CER EOS on the permeability as well as the lipid organization was studied using mixtures prepared with PCERs. As in the present study the SCSs have been prepared from natural CERs, the extrapolation of the results to the *in vivo* situation is more straight forward compared to mixtures prepared from synthetic CERs. This is especially true when varying the level of FFAs. Thus a phase transition from hexagonal to an orthorhombic lateral packing is restricted by using mixtures with

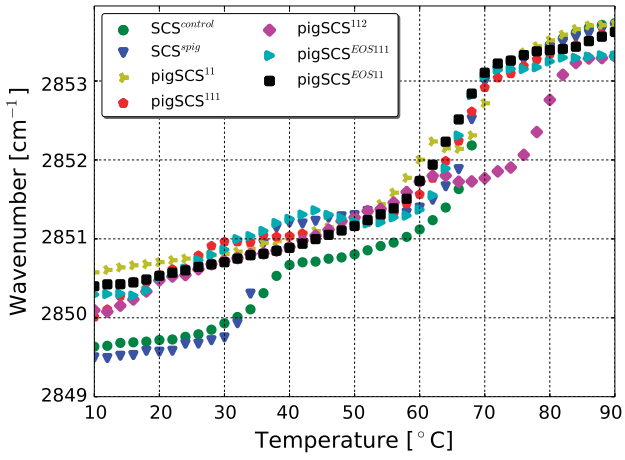

Fig. 7. The CH_2 symmetric stretching frequency thermotropic response curves for the various SCSs. The higher CH_2 symmetric stretching wavenumbers indicate higher conformational disordering values. Higher CH_2 symmetric stretching wavenumbers are observed for the SCSs prepared from PCERs while lower values are observed in the spectra of SCSs prepared from synthetic CERs.

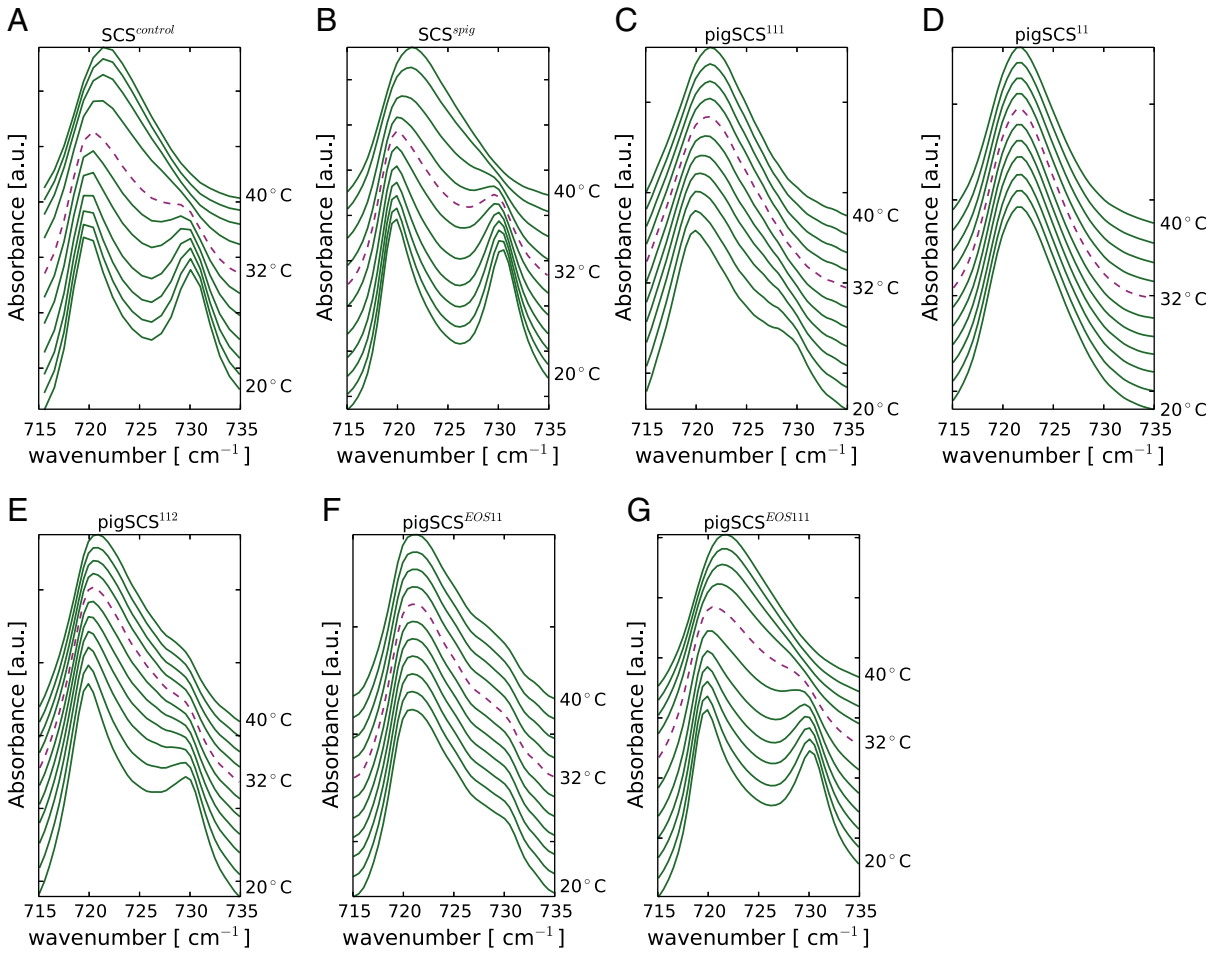

Fig. 8. Thermotropic CH_2 rocking vibration frequencies as a function of temperature for various SCSs. The spectra are shown from a 20 to 40 °C temperature region and 32 °C is highlighted as the permeation studies performed at this temperature (the skin temperature).

synthetic CERs, such as in the latter long chain FFAs with a certain chain length distribution, which are required for a proper mixing of the lipids forming the two lamellar phases. In such mixtures, however, the lipids form an orthorhombic packing. This is the reason why in previous studies the orthorhombic to hexagonal packing on the lipid barrier was studied using diffusion studies carried out as a function of temperature. These increased temperatures induce an orthorhombic to hexagonal phase transition.

4.1. CER chain length distribution affects the lipid barrier

When comparing the steady state flux of SCSs prepared from either synthetic CERs or PCERs, we do notice a significant difference: all SCSs prepared from PCER containing mixtures exhibit higher steady state fluxes than observed with SCSs prepared using synthetic CERs. When comparing the CER composition of SCS^{spig} and $pigSCS^{111}$, the CER subclass composition is very similar. However, the PCER subclasses have a wide chain length distribution whereas the synthetic CER subclasses display only three different acyl chain lengths and only a single sphingoid base length. Therefore, these studies clearly show that chain length distribution affects the permeability of the SCS quite drastically. Then the question arises, whether a wider distribution of chain lengths will affect the lamellar phases and/or the lateral organization consequently resulting in an increased steady state flux. When focusing on the lamellar phases, no drastic differences were observed between SCS^{spig} and $pigSCS^{111}$. In both SCSs, the LPP and the SPP coexist. Although the repeat distances are somewhat different, namely with a slight increase in the $pigSCS^{111}$, this is not expected to be a major factor for the increased steady state flux in the $pigSCS^{111}$. However, when we focus on the lateral packing, differences are observed. While at around 32 °C, in the SCS^{spig}, mostly an orthorhombic lateral packing is observed, in the $pigSCS^{111}$ mainly a hexagonal lateral packing prevails. In addition, at 32 °C a higher conformational disordering is noticed in the $pigSCS^{111}$ (CH_2 stretching vibrations at around 2851 cm^{-1}) compared to that in the SCS^{spig}. The higher stretching vibration frequencies perhaps indicate that, a small subpopulation of lipids may adopt a liquid phase at this temperature which may facilitate the diffusion of a hydrocortisone drug compound by increasing the conformational disordering in the lipid tails. However, at 32 °C the lamellar phases are still evident from SAXD measurements. Therefore, the liquid phase present at 32 °C is expected to be located in the lipid lamellae coexisting with the more crystalline domains. Both the presence of mainly a hexagonal lateral packing as well as an increased conformational disordering may be responsible for the increased steady state flux of the $pigSCS^{111}$ compared to the SCS^{spig}. Most probably the mismatch between the various chain lengths within the lipid lamellae is responsible for these observed differences.

4.2. Levels of FFA and CER EOS affect lipid barrier

An increased level of CER EOS or FFA in the pigSCS reduces the steady state flux and therefore increases the lipid barrier. While the levels of CER EOS and FFA were both increased two-fold, the increase in CER EOS level reduced the steady state flux most drastically. This is indicative of an increased lipid barrier of SCSs prepared from PCERs.

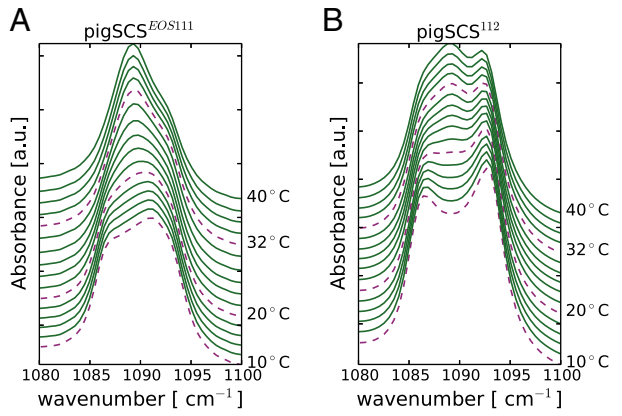

Fig. 9. FTIR spectra of the deuterated samples. (A) The CD_2 scissoring frequency of the pigSCS^{EOS111} prepared with DFFA. (B) The CD_2 scissoring frequency of the pigSCS^{112} prepared with DFFA. The absence and/or presence of a very weak doublet at 32 °C indicates that the lipids are forming a homogeneous mixture and very little lipids eventually exist as phase separated domains.

Nonetheless, both steady state fluxes are still higher than across the synthetic CER containing SCSs.

When focusing on the lamellar organization of the SCS, an increase in the level of CER EOS, i.e., pigSCS^{EOS111}, results in only the formation of the LPP. In previous studies using SCS from synthetic CERs, it was shown that an increased presence of the LPP results in a reduction in the steady state flux [25]. When focusing on the lateral organization a slight increase in the orthorhombic organization was observed at 32 °C, the temperature of the SCS during the diffusion studies, while the conformational ordering remained very similar. Therefore in case of enrichment in CER EOS, the reduced steady state flux is most probably due to both the increased formation of the LPP and the increased presence of the orthorhombic lateral packing. This is different for increased levels of FFA in the SCS. As in this pigSCS^{112} only a SPP is present. This is expected to increase the steady state flux of hydrocortisone [25]. However, in this SCS at 32 °C, a slight increase in the orthorhombic organization together with an increased conformational ordering in the CH_2 symmetric stretching vibration is observed compared to that in pigSCS^{111}. Therefore, in this case, mainly the changes in conformational ordering and lateral organization will contribute to the reduced steady state flux across the SCS, while the presence of only the SPP is expected to counteract the reduced permeability.

Very interestingly, in the FTIR spectrum of the enriched EOS containing SCSs (pigSCS^{EOS111}), the rocking vibration at 730 cm^{-1} strongly reduces when the temperature is increased, while in the FTIR spectrum of the pigSCS^{112} this is less obvious. Therefore, we wondered whether in the latter phase separation occurred between the FFA and CER as the FFA undergoes an orthorhombic to liquid phase transition at elevated temperatures and thus the shoulder at 730 cm^{-1} may be due to phase separated FFA. To examine this, measurements were performed in which the protonated FFA was replaced by the deuterated counterparts. Indeed these studies showed that in the pigSCS^{112} a fraction of the DFFA phase separates. However, most probably these DFFA phase separated domains are still within the same lipid lamellae as only one lamellar phase is detected by SAXD.

4.3. Lipid organization in SCS^{control} and SCS^{spig}

The SCS^{control} and SCS^{spig} differ very little in CER subclass composition and are almost identical. Therefore, the formation of the lamellar phases in these two mixtures is very similar as illustrated by the SAXD profiles. The FTIR measurements also revealed similar lateral packing and conformational disordering values for these two mixtures. This may indicate that, the SCSs prepared from these two lipid mixtures share the same barrier properties which were confirmed by diffusion studies: no significant differences in permeation flux have been observed between SCS^{control} and SCS^{spig}.

4.4. Comparison between present results and previously obtained data

In a previous study, we examined the lipid barrier of SCS^{control} and focused on the change of an orthorhombic–hexagonal lateral phase transition and the effect on the diffusional barrier [14]. In that previous study, we performed permeation studies as a function of temperature. From the slope of the Arrhenius plot the activation energy for diffusion was calculated. In that study no difference in the slope and thus activation energy were observed indicating no difference in diffusion between the hexagonal lateral packing (higher temperature phase and orthorhombic lateral packing (lower temperature phase). This is different from the present observation. This could have at least three reasons: i) in the previous study the model drug benzoic acid was selected, the flux of which may be less sensitive to changes in the lateral packing, ii) changes in the activation energy of diffusion were obtained from the slope of the Arrhenius plot, which is a less sensitive method than employed in the present study or iii) the solubility of benzoic acid in the hexagonal phase is higher than in the orthorhombic lateral packing, which would not affect the activation energy, but will affect the steady state flux values. In order to compare our current method with the previously employed method for benzoic acid, we have performed an additional permeation experiment taking benzoic acid as a model drug and using our current lipid mixtures namely pigSCS^{111} and pigSCS^{EOS111} with a hexagonal and orthorhombic packing, respectively. The steady state flux we obtained for pigSCS^{111} is 35.4 ± 5.9 μg/cm^2/h which is significantly higher than pigSCS^{EOS111} having a steady state flux of 25.6 ± 4.9 μg/cm^2/h. These results demonstrate that the lateral packing affects the steady state flux not only of hydrocortisone, but also of benzoic acid and that the lateral packing affects the permeability of the SCS.

4.5. The importance of chain length in maintaining the lipid barrier

Human SC prevails at a broad chain length distribution, but the population of the shorter chain CER in pig SC is elevated compared to that in human SC [23,36]. This might be the reason for the increased level of lipids forming an orthorhombic phase observed in human SC compared to pig SC [8]. However, previously we also measured mixtures of isolated pig CERs, CHOL and FFA, in which the FFA had the same composition as used in the present study. In these studies, we observed the presence of an orthorhombic packing by wide angle X-ray diffraction, but we could not examine whether a hexagonal lateral packing was also present as the single diffraction ring attributed to the hexagonal lateral packing is obscured by those of the orthorhombic packing [37]. Furthermore, since at that time the pig CER chain length was not analyzed, no information was available about chain length distribution. A difference in chain length distribution of the pig CER mixtures used in the previous and present study may affect the lateral packing. The effect of chain length distribution on the lateral packing has also been observed in clinical studies where the reduced chain length in CERs correlates with an increased presence of a hexagonal lateral packing indicative of an altered barrier [13]. Previously, we also studied the effect of reduced FFA chain length on the lipid barrier of SCS prepared with CER^{control}, CHOL and short chain FFAs [14]. These studies showed that a reduction in the FFA chain length makes the packing more hexagonal and also increases the permeation flux several fold, an indication of a reduced barrier function. However, in the latter there was also a change in the formation of the lamellar phases.

4.6. Extrapolation to the in vivo situation

The studies described in this paper show that i) a wider distribution of CER chain lengths by including CER with a shorter chain length, ii) a

reduced level of FFA or iii) a reduced level of CER EOS will reduce the lipid barrier function. As the lipid composition mimics very closely that in SC with natural CERs, we may extrapolate our finding to the *in vivo* situation. As far as the level of CER EO classes are concerned, in several studies performed with mice knockdown of the genes for the ELOVL 1, 4 and ceramide synthase 3 [20,38,39] the results show a near absence of all very long acyl CERs (CER EOS is one of these subclasses). In these mice there is a drastic increase in the permeability of the skin. Although the changes in lipid composition and organization are not the only factors that play a role in the impaired skin barrier function in these mice, the present study shows that reduced levels of acyl CERs contribute to a change in the lipid organization (reduced levels of orthorhombic packing) and subsequently an impaired skin barrier function. Patients with autosomal recessive congenital ichthyosis also suffer from an impaired skin barrier function. In these patients a reduced ceramide synthase 3 enzyme activity has also been reported together with a reduced level of acyl CERs [20]. Besides the levels of acyl CERs, a reduced level of FFAs results in an enhanced presence of the hexagonal lateral packing and a reduced lipid barrier. In the SC of lamellar ichthyosis patients reduced levels of FFAs and an increased level of lipids adopting the hexagonal lateral packing have been reported. Our present studies show using natural CERs that these changes may contribute to the impaired skin barrier function in these patients [40,41]. Another interesting group of patients with an impaired skin barrier is that of atopic dermatitis patients. Recently we observed a reduction in the average chain length of the CERs that correlated with a reduced skin barrier [13,42]. Due to a shift in the CER chain lengths toward a shorter chain length, the chain length distribution is expected to be wider than in healthy subjects. The present study shows that indeed a change in chain length distribution toward a shorter chain length may have a detrimental effect on the skin barrier function. Apart from the reduction in CER and FFA chain lengths, the increased level of unsaturated FFAs as observed in patients with atopic dermatitis and Netherton syndrome is also expected to reduce the skin barrier function [43,44]. The effect of the unsaturated FFAs on the lipid barrier is currently investigated.

5. Conclusion

Our current studies show that the permeability of SCSs prepared from PCERs is higher compared to the SCSs prepared from synthetic CERs demonstrating that a wider chain length distribution of the PCERs contributes to a reduced lipid barrier. Simultaneously the wider chain length distribution enhances the formation of a hexagonal lateral packing, and an increased conformational disordering. These changes in lipid organization may be responsible for the reduced lipid skin barrier. Increased levels of CER EOS or FFA in the pigSCSs have an opposite effect: an improve lipid barrier is monitored, simultaneously with an enhanced orthorhombic lateral packing confirming the importance of the lipid packing and ordering for the lipid barrier.

Acknowledgements

We would like to thank the company Evonik for their generous provision of CERs and the personnel at the DUBBLE beam line 26b at the ESRF located at Grenoble, France for their assistance during the X-ray diffractions measurements. We like to thank Jeroen van Smeden for his assistance and interpretation of the LC/MS results.

References

[1] P.W. Wertz, M.C. Miethke, S.A. Long, J.S. Strauss, D.T. Downing, The composition of the ceramides from human stratum corneum and from comedones, J. Investig. Dermatol. 84 (1985) 410–412.
[2] K.J. Robson, M.E. Stewart, S. Michelsen, N.D. Lazo, D.T. Downing, 6-Hydroxy-4-sphingenine in human epidermal ceramides, J. Lipid Res. 35 (1994) 2060–2068.
[3] M.E. Stewart, D.T. Downing, A new 6-hydroxy-4-sphingenine-containing ceramide in human skin, J. Lipid Res. 40 (1999) 1434–1439.
[4] M. Ponec, A. Weerheim, P. Lankhorst, P. Wertz, New acylceramide in native and reconstructed epidermis, J. Investig. Dermatol. 120 (2003) 581–588.
[5] Y. Masukawa, H. Narita, E. Shimizu, N. Kondo, Y. Sugai, T. Oba, R. Homma, J. Ishikawa, Y. Takagi, T. Kitahara, Y. Takema, K. Kita, Characterization of overall ceramide species in human stratum corneum, J. Lipid Res. 49 (2008) 1466–1476.
[6] A. Weerheim, M. Ponec, Determination of stratum corneum lipid profile by tape stripping in combination with high-performance thin-layer chromatography, Arch. Dermatol. Res. 293 (2001) 191–199.
[7] J.A. Bouwstra, G.S. Gooris, J.A. van der Spek, W. Bras, Structural investigations of human stratum corneum by small-angle X-ray scattering, J. Investig. Dermatol. 97 (1991) 1005–1012.
[8] J.A. Bouwstra, G.S. Gooris, W. Bras, D.T. Downing, Lipid organization in pig stratum corneum, J. Lipid Res. 36 (1995) 685–695.
[9] M. Boncheva, F. Damien, V. Normand, Molecular organization of the lipid matrix in intact stratum corneum using ATR-FTIR spectroscopy, Biochim. Biophys. Acta Biomembr. 1778 (2008) 1344–1355.
[10] B. Ongpipattanakul, M.L. Francoeur, R.O. Potts, Polymorphism in stratum corneum lipids, Biochim. Biophys. Acta Biomembr. 1190 (1994) 115–122.
[11] G.S.K. Pilgram, A.M.E.-V. Pelt, J.A. Bouwstra, H.K. Koerten, Electron diffraction provides new information on human stratum corneum lipid organization studied in relation to depth and temperature, 113 (1999) 403–409.
[12] J.A. Bouwstra, G.S. Gooris, M.A.S.-D. Vries, J.A. van der Spek, W. Bras, Structure of human stratum corneum as a function of temperature and hydration: a wide-angle X-ray diffraction study, Int. J. Pharm. 84 (1992) 205–216.
[13] M. Janssens, J. van Smeden, G.S. Gooris, W. Bras, G. Portale, P.J. Caspers, R.J. Vreeken, T. Hankemeier, S. Kezic, R. Wolterbeek, A.P. Lavrijsen, J.A. Bouwstra, Increase in short-chain ceramides correlates with an altered lipid organization and decreased barrier function in atopic eczema patients, J. Lipid Res. 53 (2012) 2755–2766.
[14] D. Groen, D.S. Poole, G.S. Gooris, J.A. Bouwstra, Is an orthorhombic lateral packing and a proper lamellar organization important for the skin barrier function? Biochim. Biophys. Acta Biomembr. 1808 (2011) 1529–1537.
[15] R.O. Potts, M.L. Francoeur, Lipid biophysics of water loss through the skin, Proc. Natl. Acad. Sci. 87 (1990) 3871–3873.
[16] F. Damien, M. Boncheva, The extent of orthorhombic lipid phases in the stratum corneum determines the barrier efficiency of human skin *in vivo*, J. Investig. Dermatol. 130 (2010) 611–614.
[17] J. van Smeden, L. Hoppel, R. van der Heijden, T. Hankemeier, R.J. Vreeken, J.A. Bouwstra, LC/MS analysis of stratum corneum lipids: ceramide profiling and discovery, J. Lipid Res. 52 (2011) 1211–1221.
[18] J.A. Bouwstra, G.S. Gooris, F.E.R. Dubbelaar, A.M. Weerheim, A.P. Ijzerman, M. Ponec, Role of ceramide 1 in the molecular organization of the stratum corneum lipids, J. Lipid Res. 39 (1998) 186–196.
[19] D. Groen, G.S. Gooris, D.J. Barlow, M.J. Lawrence, J.B. van Mechelen, B. Demé, J.A. Bouwstra, Disposition of ceramide in model lipid membranes determined by neutron diffraction, Biophys. J. 100 (2011) 1481–1489.
[20] R. Jennemann, M. Rabionet, K. Gorgas, S. Epstein, A. Dalpke, U. Rothermel, A. Bayerle, F. van der Hoeven, S. Imgrund, J. Kirsch, W. Nickel, K. Willecke, H. Riezman, H.-J. Gröne, R. Sandhoff, Loss of ceramide synthase 3 causes lethal skin barrier disruption, Hum. Mol. Genet. 21 (2012) 586–608.
[21] E.H. Mojumdar, D. Groen, G.S. Gooris, D.J. Barlow, M.J. Lawrence, B. Deme, J.A. Bouwstra, Localization of cholesterol and fatty acid in a model lipid membrane: a neutron diffraction approach, Biophys. J. 105 (2013) 911–918.
[22] Y.-H. Park, W.-H. Jang, J.A. Seo, M. Park, T.R. Lee, Y.-H. Park, D.K. Kim, K.-M. Lim, Decrease of ceramides with very long-chain fatty acids and downregulation of elongases in a murine atopic dermatitis model, vol. 132, Nature Publishing Group, 2012, pp. 476–479.
[23] J. van Smeden, W.A. Boiten, T. Hankemeier, R. Rissmann, J.A. Bouwstra, R.J. Vreeken, Combined LC/MS-platform for analysis of all major stratum corneum lipids, and the profiling of skin substitutes, Biochim. Biophys. Acta Mol. Cell Biol. Lipids 1841 (2014) 70–79.
[24] P.W. Wertz, D.T. Downing, P.W. Wertz, D.T. Downing, Epidermal lipids, in: L.A. Goldsmith (Ed.), Physiology, Biochemistry, and Molecular Biology of the Skin, Oxford University Press, New York, 1991, pp. 205–236.
[25] M. Jager, W. Groenink, R. Bielsa, I. Guivernau, E. Andersson, N. Angelova, M. Ponec, J. Bouwstra, A novel in vitro percutaneous penetration model: evaluation of barrier properties with P-aminobenzoic acid and two of its derivatives, Pharm. Res. 23 (2006) 951–960.
[26] M. de Jager, W. Groenink, J. van der Spek, C. Janmaat, G. Gooris, M. Ponec, J. Bouwstra, Preparation and characterization of a stratum corneum substitute for *in vitro* percutaneous penetration studies, Biochim. Biophys. Acta Biomembr. 1758 (2006) 636–644.
[27] J.A. Bouwstra, G.S. Gooris, K. Cheng, A. Weerheim, W. Bras, M. Ponec, Phase behavior of isolated skin lipids, J. Lipid Res. 37 (1996) 999–1011.
[28] E.G. Bligh, W.J. Dyer, A rapid method of total lipid extraction and purification, Can. J. Biochem. Physiol. 37 (1959) 911–917.
[29] M.W. de Jager, G.S. Gooris, M. Ponec, J.A. Bouwstra, Lipid mixtures prepared with well-defined synthetic ceramides closely mimic the unique stratum corneum lipid phase behavior, J. Lipid Res. 46 (2005) 2649–2656.
[30] P.W., Epidermal lipids, Physiology, Biochemistry and Molecular Biology of the Skin, Oxford University Press, Oxford, 1991.
[31] D. Groen, G.S. Gooris, M. Ponec, J.A. Bouwstra, Two new methods for preparing a unique stratum corneum substitute, Biochim. Biophys. Acta 1778 (2008) 2421–2429.

[32] A. Di Nardo, P. Wertz, A. Giannetti, S. Seidenar, Ceramide and cholesterol composition of the skin of patients with atopic dermatitis, Acta Derm. Venereol. 78 (1998) 27–30.
[33] D.J. Moore, M.E. Rerek, R. Mendelsohn, FTIR spectroscopy studies of the conformational order and phase behavior of ceramides, J. Phys. Chem. B 101 (1997) 8933–8940.
[34] R. Mendelsohn, G.L. Liang, H.L. Strauss, R.G. Snyder, IR spectroscopic determination of gel state miscibility in long-chain phosphatidylcholine mixtures, Biophys. J. 69 (1995) 1987–1998.
[35] R.G. Snyder, M.C. Goh, V.J.P. Srivatsavoy, H.L. Strauss, D.L. Dorset, Measurement of the growth kinetics of microdomains in binary n-alkane solid solutions by infrared spectroscopy, J. Phys. Chem. 96 (1992) 10008–10019.
[36] P.W. Wertz, D.T. Downing, Ceramides of pig epidermis: structure determination, J. Lipid Res. 24 (1983) 759–765.
[37] J.A. Bouwstra, G.S. Gooris, F.E.R. Dubbelaar, A.M. Weerheim, M. Ponec, pH, cholesterol sulfate, and fatty acids affect the stratum corneum lipid organization, J. Investig. Dermatol. Symp. Proc. 3 (1998) 69–74.
[38] V. Vasireddy, Y. Uchida, N. Salem, S.Y. Kim, M.N.A. Mandal, G.B. Reddy, R. Bodepudi, N.L. Alderson, J.C. Brown, H. Hama, A. Dlugosz, P.M. Elias, W.M. Holleran, R. Ayyagari, Loss of functional ELOVL4 depletes very long-chain fatty acids (≥C28) and the unique ω-O-acylceramides in skin leading to neonatal death, Hum. Mol. Genet. 16 (2007) 471–482.
[39] T. Sassa, Y. Ohno, S. Suzuki, T. Nomura, C. Nishioka, T. Kashiwagi, T. Hirayama, M. Akiyama, R. Taguchi, H. Shimizu, S. Itohara, A. Kihara, Impaired epidermal permeability barrier in mice lacking elovl1, the gene responsible for very-long-chain fatty acid production, Mol. Cell. Biol. 33 (2013) 2787–2796.
[40] A.P. Lavrijsen, J.A. Bouwstra, G.S. Gooris, A. Weerheim, H.E. Boddé, M. Ponec, Reduced skin barrier function parallels abnormal stratum corneum lipid organization in patients with lamellar ichthyosis, J. Investig. Dermatol. 105 (1995) 619–624.
[41] G.S.K. Pilgram, D.C.J. Vissers, H. van der Meulen, S. Pavel, S.P.M. Lavrijsen, J.A. Bouwstra, H.K. Koerten, Aberrant lipid organization in stratum corneum of patients with atopic dermatitis and lamellar ichthyosis, 117 (2001) 710–717.
[42] J. Ishikawa, H. Narita, N. Kondo, M. Hotta, Y. Takagi, Y. Masukawa, T. Kitahara, Y. Takema, S. Koyano, S. Yamazaki, A. Hatamochi, Changes in the ceramide profile of atopic dermatitis patients, J. Investig. Dermatol. 130 (2010) 2511–2514.
[43] J. van Smeden, M. Janssens, E.C.J. Kaye, P.J. Caspers, A.P. Lavrijsen, R.J. Vreeken, J.A. Bouwstra, The importance of free fatty acid chain length for the skin barrier function in atopic eczema patients, Exp. Dermatol. 23 (2014) 45–52.
[44] J. van Smeden, M. Janssens, W.A. Boiten, V. van Drongelen, L. Furio, R.J. Vreeken, A. Hovnanian, J.A. Bouwstra, Intercellular skin barrier lipid composition and organization in Netherton syndrome patients, J. Investig. Dermatol. 134 (2013) 1238–1245.